Out-of-Plane Non-linear Warping of a Slice into Volume[1]

Boklye Kim, Jennifer L. Boes, Peyton H. Bland, and Charles R. Meyer

Department of Radiology
University of Michigan Medical Center
Ann Arbor, Michigan, 48109-0553 USA
[1]boklyek@umich.edu
http://www.med.umich.edu/dipl/

Abstract. Non-linear 3D warping is implemented for registration of a planar (2D) image into an anatomical reference volume space for accurate spatial mapping. The mutual information based automatic warping algorithm is expanded to include the 2D-to-3D mapping of slice images exhibiting localized out-of-plane geometric deformations. Presented in this work is demonstration and evaluation of the control point based 3D thin-plate-spline (TPS) function applied to the correction of local deformations in MR slice images. Automated 3D warping of a slice into an anatomical reference volume space is achieved by optimization of the mutual information cost function calculated from the gray values of the image pair, i.e., the reference volume and a slice. Accuracy in spatial mapping was assessed by using the simulated MR data sets in a standard anatomical coordinate system and locally induced deformations in a slice image with known TPS transformation parameters. The results indicate the sensitivity of the final optimization to DOF and selected control point locations.

1. Introduction

Recently, we have demonstrated the capability of retrospectively mapping a slice image into an anatomical reference volume from the same subject using a simple rigid body transformation of six degrees of freedom (DOF) [1]. The mapping is achieved by an automated registration routine driven by a cost metric calculated from the global mutual information of the two volume data [2, 3]. In practice, correction of 2D image deformations is often presented as a non-linear warping problem that is not limited to the imaging plane. Out-of-plane warp, typically encountered in multislice MRI data series, is the local field induced deformations induced by the gradient field or susceptibility effect, or localized out-of-plane motion artifacts [4, 5]. This research

[1] This research was supported in part by DHHS NIH 2R01 CA59412-04A1

C. Taylor, A. Colchester (Eds.): MICCAI'99, LNCS 1679, pp. 638 -646, 1999.

is focused on correcting the 3D warping artifacts localized in the brain regions that undergo physiological motion, i.e., brain stem, due to the cardiac cycle.

We have expanded the mutual information based automatic registration capability for correction of planar image data exhibiting geometric distortions that include out-of-plane and non-linear warping. The control point based thin-plate-spline (TPS) function is applied to the correction of the local deformations. The non-linear warping capability of TPS can be efficient for correcting local, 3D deformations [6, 7]. In regions distant from the control points, the solution becomes an affine (linear) transformation while its warping effects are limited to local regions. It is beneficial for this 2D-to-3D warping to respond to the 3D deformations locally and not affect other regions that require different solutions.

Initial homologous control points are obtained by the user marking the approximate locations in each data set. The degrees of freedom (DOF) in the solution is controlled by the number of homologous points used. Selecting one point more than the spatial dimension constrains the solution to the affine transformation while selecting additional points implements a general TPS warping solution. Since these control points drive the optimization, the number of variables to optimize is the product of the number of points and the number of spatial dimensions. The initial state vector contains the coordinates of the selected points that define the geometric mapping.

Presented in this paper are demonstration and evaluation of 3D warping of a slice image (2D) into a reference volume space. Accuracy of the spatial mapping was assessed by using simulated MR data sets in a standard anatomical coordinate system and local deformations induced by a known set of TPS transformation parameters.

2 Methods

A slice image taken out of the simulated volumetric brain MRI data from International Consortium of Brain Mapping (ICBM) was used to demonstrate the 3D non-linear warping of a slice image [8]. The localized out-of-plane warping artifact was induced to mimic the brain stem movement effect in slice images during the multislice single shot Echo-Planar imaging (EPI) acquisition [9, 10]. Slice images acquired from a volume containing non-stationary structures, i.e., squeezing of ventricles or brain stem movement, need nonlinear solutions to relocate the voxels to their actual positions at the time of the acquisition. For axial slices the brain stem motion would cause an out-of-plane systematic distortion, i.e., funnel effect. Use of a brain model and simulated local brain motion artifact provide the geometric truth for the warping solution.

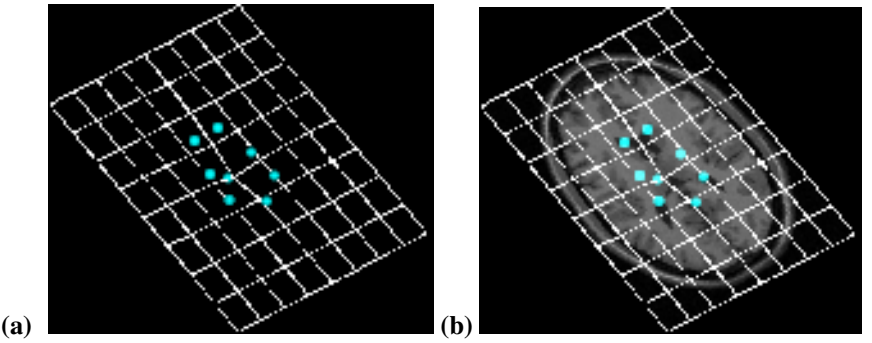

Fig.1. (a) An out-of-plane local warp, i.e., funnel effect, produced by the eight control point 3D TPS function with one homologous point (center) displaced out of the plane. (b) The planar image reconstructed from a T_1-weighted MRI volume using the warping function contains out-of-plane features.

2.1 Locally Warped Planar Image

Out-of-plane warping was created by mapping eight control point sets in a pair of volumetric image data set using a TPS function. One point in the homologous control point set was displaced by 4 mm out of the image plane to induce the funnel effect. Figure 1 shows the local 3D funnel effect deformation in a slice image. The local out-of-plane warp is depicted by (a) the grid mesh and (b) superimposed on the slice image.

2.2 Automated 3D Unwarping of a Slice into Volume

The automated registration of a warped T_1-weighed MRI slice in Fig.1(b) into a reference volume space, T_2-weighted MRI volume data, was achieved by allowing the optimizer to move the control points in the homologous 3D space to positions that minimize the MI cost function calculated from the gray values of the image pair. The mutual information metric (MI = -mutual information) and Mutual Information Automated Multimodality Image Fusion (MIAMI Fuse) software were presented previously for spatial mapping of multimodal image data sets [2, 3, 11].

The registration process is an iterative method driven by MI cost metric and the Nelder-Mead downhill simplex optimization algorithm was implemented [12]. The optimization routine determines the transformation coefficients for a coordinate mapping using either affine or TPS warp transformation and performs trilinear interpolation to map gray scale values of the image voxels. The MI cost metric is computed from the voxel/pixel gray values in the reconstructed data set, therefore, the effect of the geometric mapping is manifested. The trilinear interpolation process uses the original data set for each iteration instead of using the previous interpolation

to generate the successive data. This approach prevents round-off and other undesired interpolation effects such as smoothing from accumulating across iterations.

Each optimization cycle is initiated by a random perturbation of the initial transformation vector. During the iteration, the optimizer moves the control points by small increments in an orderly fashion within the given radial bound. At each configuration of the control points, the data sets are mapped, and the resulting MI is computed. The optimizer keeps a history of control point positions and MI values to allow it to move toward an optimal control point configuration. Each iteration was set to stop when movement of control points is < 0.01 mm and the optimization cycle was repeated till the $\Delta MI < 0.00001$ for successive cycle.

3 Results

3.1. 2D-to-3D Warping Accuracy

The registration accuracy of a slice into the reference volume using the 3D TPS function with random displacement of the initial vector was evaluated. Figure 2 shows the resulting out-of-plane warp of the slice mapped into the anatomical volume space using TPS function defined by the coordinates of the final optimized vector. The slice exhibiting the local warp is reconstructed in the reference space (Fig. 2a) and superimposed on the reference volume data as displayed in a coronal view (Fig. 2b). The effect of the 3D unwarping the funnel effect artifact is demonstrated by the planar visualization of the selected slices from the final reconstructed volume data and the corresponding slices from the reference data in Fig. 2c and Fig.2d,respectively.

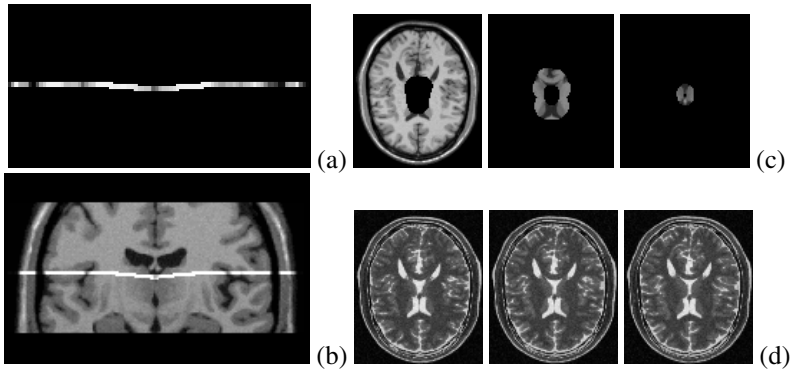

Fig. 2. Pictorial presentation of the resulting 3D warping of a slice image into a volume. The acquired slice image reconstructed into the volume is indicated by the high intensity lines in coronal views (a) and (b). The planar axial images show the warping of a (c) slice with a 3D deformation reconstructed into a reference volume and (d) the corresponding reference images.

Table 1. The average and standard error (STE) of the final mapping error of the eight control points relative to the truth.

control points	average	STE
1	0.51063484	0.06689679
2	0.43713253	0.06933018
3	0.51385107	0.07932435
4	0.71478606	0.11352397
5	1.30181737	0.24647948
6	0.40896756	0.05031346
7	0.42290929	0.09483279
8	0.51820495	0.12233572

The averaged error of the solution was calculated for the final stopping positions of the eight control points over five optimizations with the initial search bound of 20 mm (=20 voxels). The error was assessed by computing the average and standard rms error (STE) of the control points with respect to the true solution as listed in Table 1. The averaged rms of the mapping coordinates and STE over all the points were 0.56±0.04.

3.2 2D-to-3D Warping as a Function of DOF

The mapping accuracy of the 3D TPS solutions for correction of the out-of-plane local warping in the slice image was evaluated as a function of number of control points. The registration was performed using sets of 4 to 10 control point points. The plot of MI cost metric versus number of control points in Fig. 3 displays the dependence of the final MI as a function of DOF. The plot indicates the optimal, i.e., minimum, MI with eight control points and increase in MI with the overshoot of DOF. For each number of control point set, the original eight homologous control points were mapped back into the reference space using the final transformation to determine the registration error. The transformed positions of the eight control points were used to compute the rms error of the coordinate displacement from the original eight points of the geometric truth. The plot of the average rms of the displacement over eight control points versus number of control points, Fig.4, demonstrates the geometric mapping as a function of DOF. Noteworthy is the sharp drop in MI values between the affine (four points) and warping starting at five points in Fig.3.

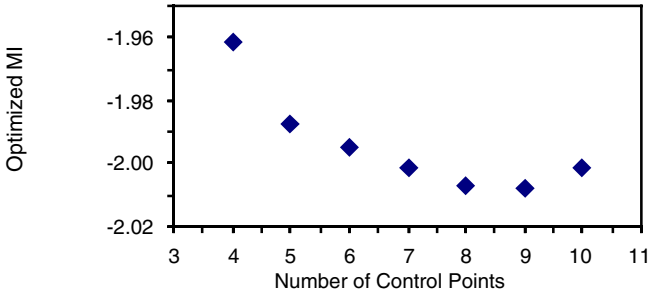

Fig.3. Plot of the final cost function versus number of control points.

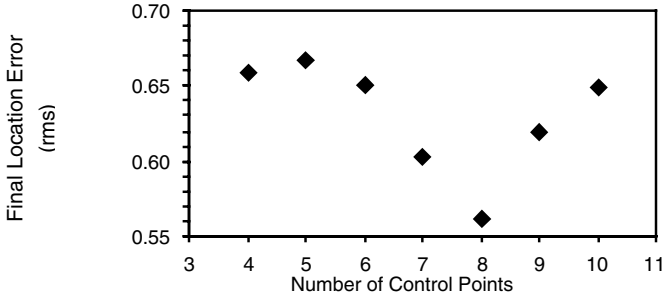

Fig.4. Plot of the final control point position rms error relative to the original positions.

3.3. 2D-to-3D Warping as a Function of Control Point Selection

Performance of the non-linear 3D registration as a function of the initial control point selection was evaluated by the final optimized MI and mapping coordinates with respect to the true solution. The TPS warp was performed using eight control points with one point selected at a position different from the original location (point 8 in Table 1). The plots in Fig.5 and 6 show the behavior of TPS warping as a function of selected control point position. The plots were constructed by moving the displaced control point in a diagonal planar direction, i.e., toward (+15 mm) and away (-15 mm) from the center of the image. The rms of the final location error and optimized MI averaged over five optimizations are plotted versus the position of the displaced control point, as shown in Fig.5 and Fig.6, respectively.

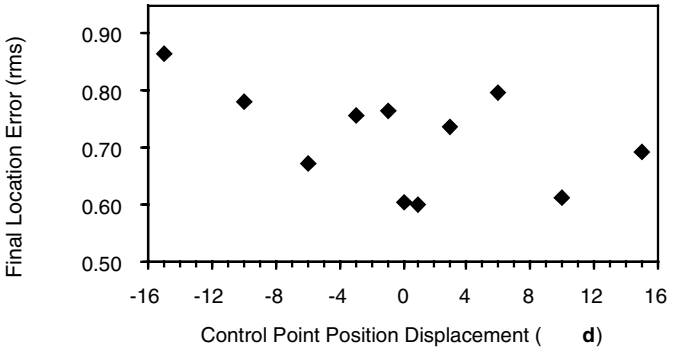

Fig. 5. Plot of averaged rms of the final position errors versus control point displacement (**d**) along the diagonal planar direction. Negative and positive signs of **d** indicate direction "away from" and "toward" the center of the image, respectively, from the original position.

Table 2. Mapping error (rms) as a function of control point position.

d (mm)	average error	STE
-15	0.8667	0.1176
-10	0.7803	0.0883
-6	0.6728	0.0787
-3	0.7581	0.0907
-1	0.7669	0.0804
0	0.6035	0.0571
1	0.5993	0.0677
3	0.7351	0.0784
6	0.7980	0.0928
10	0.6128	0.0683
15	0.6923	0.1046

4 Discussion/Conclusions

Mapping of a 2D image into a 3D volume space to correct the out-of-plane non-linear deformations present in the 2D image has been demonstrated using the TPS warping function. The test data sets provided the geometrical truth and sufficient spatial information content to drive the optimization to convergence. With the known geometric deformation parameters defined by the control point driven TPS function, the warping of a slice image was evaluated as functions of number and of position of the selected control points. There is an accurate correlation in optimization pattern between the final MI cost metric and position error as a function of number of control

points. A sharp decrease in final MI is observed between the affine solution and TPS of five control points in Fig.3. The corresponding spatial displacement error relative to the original control point positions, in Fig.4, may not represent the accurate mapping error for the case of affine transform and marks the limit to an affine solution for solving warping problems. At the other end of the series, the plots in Figs. 3 and 4 demonstrate that using more DOF than the true solution may result in less reliable registration at higher computational cost. Warping as a function of selected position of the control points was demonstrated in Fig.5 and Fig.6 with respect to the final spatial mapping and MI cost metric. Both curves indicate the presence of local minima, i.e., at positions **d** = -6 and 10. The standard errors, at the local minima, though, are greater than the global minimum at the original spatial coordinate (**d** =0) as listed in Table 2. The significance of this work is the 2D-to-3D spatial warping capability by treating the slice image deformations as 3D warping problems without the need of exclusive conditionals.

Problem of non-linear 3D distortions are commonly encountered in MR images acquired using fast imaging sequences. This work is focused on the effect of physiological brain motion, i.e. brain stem movement from the cardiac acceleration, as often observed in single shot EPI acquisition protocol [9, 10]. Such motion related artifacts pose problems for activation studies using functional MRI (fMRI) technique. Accurate geometric mapping is critical for accurate analysis of fMRI time series data since the activation detection is based on the differences in voxel intensities between the images from task-on and -off cycle assuming consistent voxel locations. In addition, fMRI is susceptible to spatial out-of-plane distortions from the field variation induced by the magnetic susceptibility as well as bulk head motion [5, 13]. This study demonstrates the feasibility of the 3D warping for accurate geometric mapping of multislice functional MR images that exhibit non-linear distortions.

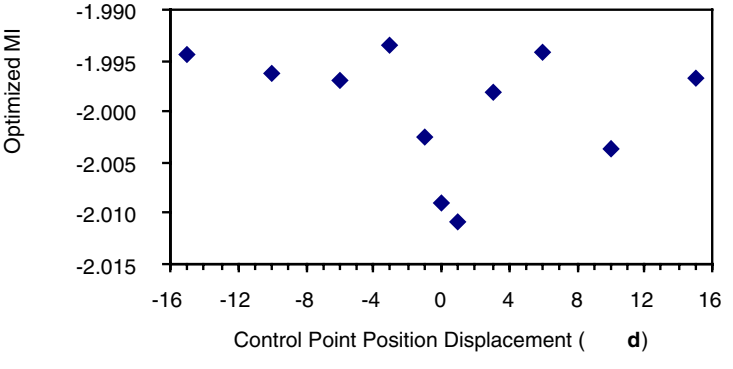

Fig.6. Plot of averaged MI versus location of control point, 8 (Table 1), indicated by the displacement amount (**d**). The original location is indicated by **d**=0.

References

1. Kim, B., *et al.*, Motion Correction in fMRI via Registration of Individual Slices into an Anatomical Volume. *Magn. Reson. Med.*, 1999, **41**(5): p 964-972.
2. Kim, B., *et al.*, Mutual information for automated unwarping of rat brain autoradiographs. *NeuroImage*, 1997. **5**(1): p. 31-40.
3. Meyer, C.R., *et al.*, Demonstration of accuracy and clinical versatility of mutual information for automatic multimodality image fusion using affine and thin plate spline warped geometric deformations. *Medical Image Analysis*, 1997. **3**: p. 195-206.
4. Jezzard, P. and R.S. Balaban, Correction of Geometric Distortion in Echo Planar Images from B0 Field Variations. *Magn. Reson. Med.*, 1995. **34**: p. 65-73.
5. Sumanaweera, T.S., *et al.*, MR Susceptibility Misregistration Correction. *IEEE Trans. Med. Img*, 1993. **12**(2): p. 251-9.
6. Bookstein, F.L., *Thin-plate Splines and the Atlas Problem for Biomedical Images*. 1991, Berlin: Springer.
7. Bookstein, F. and W.D.K.A. Green , A feature space for edgels in images with landmarks. *J of Math. Imag. and Vision*, 1993. **3**: p. 231-261.
8. Cocosco, C.A., *et al.*, BrainWeb: Online Interface to a 3D MRI Simulated Brain Database. *NeuroImage*, 1997. **5**(no.4, part 2/4): p. S425.
9. Maier, S.E., C.J. Hardy, and F.A. Jolesz, Brain and Cerebrospinal Fluid Motion: Real-Time Quantification with M-Mode MR Image. *Radiology*, 1994. **193**: p. 477-483.
10. Poncelet, B.P., *et al.*, Brain parenchyma motion: measurement with Cine Echo-planar MR imaging. *Radiology*, 1992. **185**: p. 645-651.
11. Collignon, A., *et al.* Automated multimodality image registration using information theory. *Pro. Computational Imaging and Vision.* 1995. Ile de Berder, FR: Kluwer Academic Publishers.
12. Press, W.H., *et al.*, *Numerical Recipies in C: The Art of Scientific Computing.* 1988, Cambridge: Cambridge Press. p. 305-309.
13. Weisskoff, R.M., *et al.*, Microscopic susceptibility variation and transverse relaxation: theory and experiment. *Magn. Reson. Med.*, 1994. **31**: p. 601-61-.